Water Vapor Feedbacks in the ECMWF Reanalyses and Hadley Centre Climate Model

A. SLINGO, J. A. PAMMENT, R. P. ALLAN, AND P. S. WILSON

Hadley Centre for Climate Prediction and Research, The Met. Office, Bracknell, Berkshire, United Kingdom

(Manuscript received 11 March 1999, in final form 2 September 1999)

ABSTRACT

Many studies have been made of the water vapor feedback, in both satellite data and climate model simulations. Most infer the magnitude of the feedback from the variability present in geographical distributions of the key variables, or from their seasonal variations, often using data only over the oceans. It is argued that a more direct measure of the feedback should come from the interannual variability of global mean quantities, because this timescale and space scale is more appropriate for such a global phenomenon. To investigate this suggestion, the feedback derived from the simulations of clear-sky longwave fluxes (CLERA), which used data from the 15-yr reanalysis project of the European Centre for Medium-Range Weather Forecasts, is compared with simulations by the latest version of the Hadley Centre climate model. Results are taken from an integration of the atmosphere-only version of the climate model with prescribed sea surface temperatures, as well as from a control and a global warming simulation by the coupled ocean–atmosphere version. There is broad consistency between the results from CLERA and the climate model as to the strength of the feedback, although there is considerable scatter in the CLERA results. The signal of changes in the well-mixed greenhouse gases is weak in CLERA but is dominant in the global warming simulation and has to be removed in order to diagnose the water vapor feedback. This result has implications for the exploitation of long time series of satellite and other data to study this and other feedbacks.

1. Introduction

The water vapor feedback has long been recognized to be one of the most important factors that contribute to the greenhouse effect of the earth (Arrhenius 1896; Manabe and Wetherald 1967). Observational studies of the feedback have been stimulated by the availability of satellite data, in particular radiation budget measurements from the Earth Radiation Budget Experiment (ERBE) and retrievals of column water vapor (CWV) from microwave radiometers. Raval and Ramanathan (1989) and Stephens and Greenwald (1991) studied the geographical distributions of these data over the oceans and showed that the clear-sky greenhouse effect was an increasing function of both the CWV and sea surface temperature (SST), as expected from a positive water vapor feedback. The relationship between the clear-sky greenhouse effect and SST found by Raval and Ramanathan (1989) is also consistent with that obtained in an intercomparison of general circulation models (Cess et al. 1990), from which Cess (1989) concluded that the water vapor feedback operates in a broadly similar way in the models and in reality.

Corresponding author address: Dr. Anthony Slingo, Hadley Centre, The Met. Office, London Road, Bracknell, Berkshire RG12 2SY, United Kingdom.
E-mail: aslingo@meto.gov.uk

Many subsequent papers have continued to use the geographical distributions of the clear-sky greenhouse effect, water vapor, and SST to infer the characteristics of the water vapor feedback, either from the distributions themselves or from their seasonal or interannual variability (e.g., Duvel and Bréon 1991). Attempts have also been made to derive the feedback from the changes associated with El Niño. However, there are potential drawbacks to all of these studies, which may weaken the applicability of the results to the global warming problem. First, the geographical distributions are strongly influenced by the atmospheric circulation, especially in the Tropics (Bony et al. 1997), so the spatial relationships between the key variables at a given time may not provide a reliable indication of the temporal relationships that are more relevant on the timescale of global warming. For example, El Niño is associated with large-scale changes in the tropical circulation which redistribute water vapor both in the vertical and horizontal. The effect of such changes must be removed if the signal of the water vapor feedback is to be recovered from data for limited geographical regions (Lau et al. 1996; Soden 1997). Second, all of these studies used data over the oceans only and so they are not directly comparable with the analysis of Cess et al. (1990), which inferred the feedback from changes in the global means.

Recognizing these issues, Inamdar and Ramanathan (1998) employed several datasets to extend the analysis

of the water vapor feedback to the global domain. They illustrated the importance of the dynamical redistribution of water vapor in determining the spatial pattern of the feedback. They compared the magnitude of the feedback derived from both the geographical distributions and seasonal variations and showed that they were consistent with each other and with previous estimates from both observations and climate models. The important differences between the behavior of the feedback in the Tropics compared with the whole globe, as well as between the oceans and continents, were also studied.

An alternative strategy for establishing the realism of the water vapor feedback in climate models would be to use the natural variability of the climate system on the annual and longer timescales to derive the relationships between the global means of the key variables and to compare these with estimates from observations. Cess et al. (1990) showed that climate feedbacks can be most succinctly defined in terms of global mean quantities, which therefore provide the most direct test of the sensitivity of climate models to radiative forcing. A further advantage of using global means is that they average over the geographical detail shown for example by Inamdar and Ramanathan (1998). It is of course important to study this detail in order to come to a better understanding of how changes in the atmospheric circulation control the geographical distributions of water vapor and the greenhouse effect. Indeed, such studies are a vital part of the process of understanding the internal workings of the climate system. However, for a feedback to contribute to the overall sensitivity of the system to an external forcing, on timescales relevant to global warming, it must be discernable in global mean quantities, whatever the geographical detail. In this study, we therefore deliberately avoid looking at geographical distributions and concentrate instead on global mean quantities. Some reasons why this approach has not been followed is that the satellite retrievals of CWV are only available over the oceans and that observational estimates of land surface temperatures are less reliable than those of SSTs (Slingo et al. 1998; Inamdar and Ramanathan 1998). There are also substantial areas of missing data in the ERBE clear-sky fluxes over land. In addition, most satellite datasets are only available for a few years and so provide only limited information on the variability of global mean quantities on timescales of a year or longer. Given the limitations of individual satellite datasets, it is worth investigating whether the products from recent reanalysis projects can be used in such an investigation. This was one of the motivations for performing global simulations of the clear-sky longwave fluxes using data for 1979–93 from the European Centre for Medium-Range Weather Forecasts (ECMWF) reanalyses (ERA) in the ''clear-sky longwave from ERA'' project (CLERA) (Slingo et al. 1998). The CLERA simulations provide a consistent database with which to study the clear-sky greenhouse effect and to evaluate models.

In this paper, we use results from CLERA as a surrogate for the global observations required to implement the above strategy. We are mindful of the fact that both the Re-Analyses and CLERA are based not only on observations but also on substantial modeling, but one purpose of this study is to demonstrate what might be achieved in the future if global observing systems were able to provide the same information with a minimum of modeling. The water vapor feedback is inferred from the monthly and interannual variability of the global means over the 15-yr period, an approach that is close to that used by Cess et al. (1990). The results are compared with simulations by the latest version of the Hadley Centre Climate Model, firstly from simulations by the atmosphere-only version (forced by the observed SSTs for the same period as in CLERA) and secondly from climate-prediction experiments with the coupled ocean–atmosphere version. By comparing results from these two versions with CLERA we are able to compare directly the global water vapor feedback operating in the coupled model with that in the atmosphere-only integrations.

It is important to recognize that our analysis, in common with all other studies that use observations, cannot measure the water vapor feedback *directly,* because to do that would require a controlled experiment in which one and only one variable was allowed to change at a time, thus isolating the individual partial derivatives. We can only observe the effect of the feedback *indirectly,* through its influence on the variables that are studied. In that case, many other interactions are taking place, so that only total derivatives can be derived. However, the feedback is sufficiently strong that the total derivatives provide compelling evidence for the existence of a strong, positive water vapor feedback. Nevertheless, it is important to recognize the semantic distinction between a direct measure of the feedback, derived from a controlled experiment, and the indirect measure obtained from the data analyzed in this work.

2. CLERA and climate model simulations

In the CLERA project, simulations of the clear-sky longwave radiative fluxes and heating rates were performed using data from the ECMWF reanalysis project. This provided a consistent, global dataset every 6 h for the 15 yr of the ERA period (1979–93). Details and results are discussed by Slingo et al. (1998).

An important issue with regard to the ERA data is the extent to which the signal of the water vapor feedback is due to the observations, as opposed to the model used in the assimilation. This is particularly important in the present study, since the signal is extracted from the small interannual variability of global mean quantities, as opposed to the much larger geographical variability used in most previous studies. The moisture data in ERA come primarily from radiosondes and from the one-dimensional variational assimilation (1DVAR) of

Television and Infrared Observation Satellite (TIROS) Operational Vertical Sounder (TOVS) radiances. McNally and Vesperini (1996) showed that 1DVAR produced significant improvements in the quality of the moisture analysis, compared both with radiosonde data and with independent estimates of the total column water vapor derived from the special sensor microwave/imager (SSM/I) instrument. These improvements largely removed the systematic errors in the tropical humidity distribution produced by the model. The extensive statistics shown by Uppala (1997) also demonstrate the improved fit to the moisture data in the analyses compared with the first guess from the model. While by no means definitive, these results suggest that the analyses are at least of sufficient quality to merit their use in the present study, with the caveat that comparisons with other independent sources of moisture data are needed, in particular to assess the vertical distribution of moisture in ERA and its temporal and spatial variability.

Results are also taken from the latest version of the Hadley Centre Climate Model. The atmospheric component used in integrations with prescribed SSTs is known as the Hadley Centre Atmospheric Model, version 3 (HadAM3) and the coupled model used in climate prediction experiments is known as the Hadley Centre Coupled Model, version 3 (HadCM3). Many features of the model are the same as those of an earlier version described by Johns et al. (1997), with the major exceptions that the atmospheric model now includes the Edwards and Slingo (1996) radiation code, there is a new land surface scheme (Cox et al. 1999) and the effects of convective momentum transport are included (Gregory et al. 1997). Pope et al. (2000) describe HadAM3 and the impact of the new physical parametrizations on its performance. Gordon et al. (2000) provide a description of HadCM3. The coupled model is run without flux adjustments and the control integration is extremely stable (the global average annual mean near-surface air temperature drifts by only -0.011 kelvin per century during 1000 yr of integration).

For HadAM3, results are shown from an Atmospheric Model Intercomparison Project (AMIP) integration of the model, forced by the observed SSTs for 1979–88 (Gates 1992). For HadCM3, we use results for 1950–2050 from both a control integration (Gordon et al. 2000) and from an integration with increasing concentrations of greenhouse gases, referred to henceforth as GHG (Mitchell et al. 1998). This used initial conditions appropriate for 1860 and historical concentrations of greenhouse gases up to 1990, after which the Intergovernmental Panel on Climate Change (IPCC) IS95a scenario was followed up to 2100. This integration provides valuable insights into the long-term changes in the radiation budget during global warming.

3. Results

We first compare the relationships between the CWV, clear-sky greenhouse effect, and surface temperature, derived from their geographical distributions, with previous work. The normalized clear-sky greenhouse effect g is calculated as the difference between the emission from the surface and that leaving the top of the atmosphere, divided by the emission from the surface. This normalization removes the strong dependence on temperature that would otherwise dominate the correlations and mask the signal of the water vapor feedback (Raval and Ramanathan 1989). Figures 1 and 2 show the results from CLERA and HadAM3, respectively, using data over the ice-free oceans only. Each point represents the average values in a grid box for April 1985. The character of these plots is very similar to those shown by Raval and Ramanathan (1989), Stephens and Greenwald (1991), and Duvel and Bréon (1991). The positive slopes on such figures were interpreted by these authors as evidence of a positive water vapor feedback. The slopes of the regressions provide a quantitative measure of the strength of this feedback and the values of the slopes from CLERA and HadAM3 are similar to those found in the earlier studies (Table 1).

As noted in the introduction, it is not obvious that the nature of the feedback derived from such figures is directly relevant to the case of global warming, since the latter involves the temporal behavior of the key variables as opposed to the geographical behavior shown in Figs. 1 and 2. There is also clear evidence of the effect of the atmospheric circulation, particularly at the higher SSTs. For example, the normalized greenhouse effect increases dramatically as the SSTs exceed about 300 K, as one moves from the subtropics where the troposphere is dried by subsidence to the Intertropical Convergence Zone where the upper troposphere is moistened by deep convection (Soden and Fu 1995). The slopes in this region are thus controlled mainly by the atmospheric circulation and cannot be projected to infer the change in the greenhouse effect that would occur as SSTs increase with global warming (Duvel and Bréon 1991).

A more reliable indication of the feedbacks on longer timescales should be provided by the interannual variability of global mean quantities. The rationale is that such a timescale is long compared with that over which atmospheric water vapor equilibrates with surface temperatures (estimated to be 10–30 days), but short compared with the timescale over which the radiative forcing changes due to increases in greenhouse gases. In essence, we use the natural variations in global mean surface temperature to explore a small distance along the trajectory that we believe is being followed during global warming. Unfortunately, the ERBE data cannot be used for this purpose since they were obtained for only 5 yr and contain significant regions of missing data over land areas. Instead, the CLERA simulations are used, bearing in mind the limitations in the ERA data identified by Slingo et al. (1998) and others. As will be seen, the interannual variations are extremely noisy, but some coherent signals do emerge.

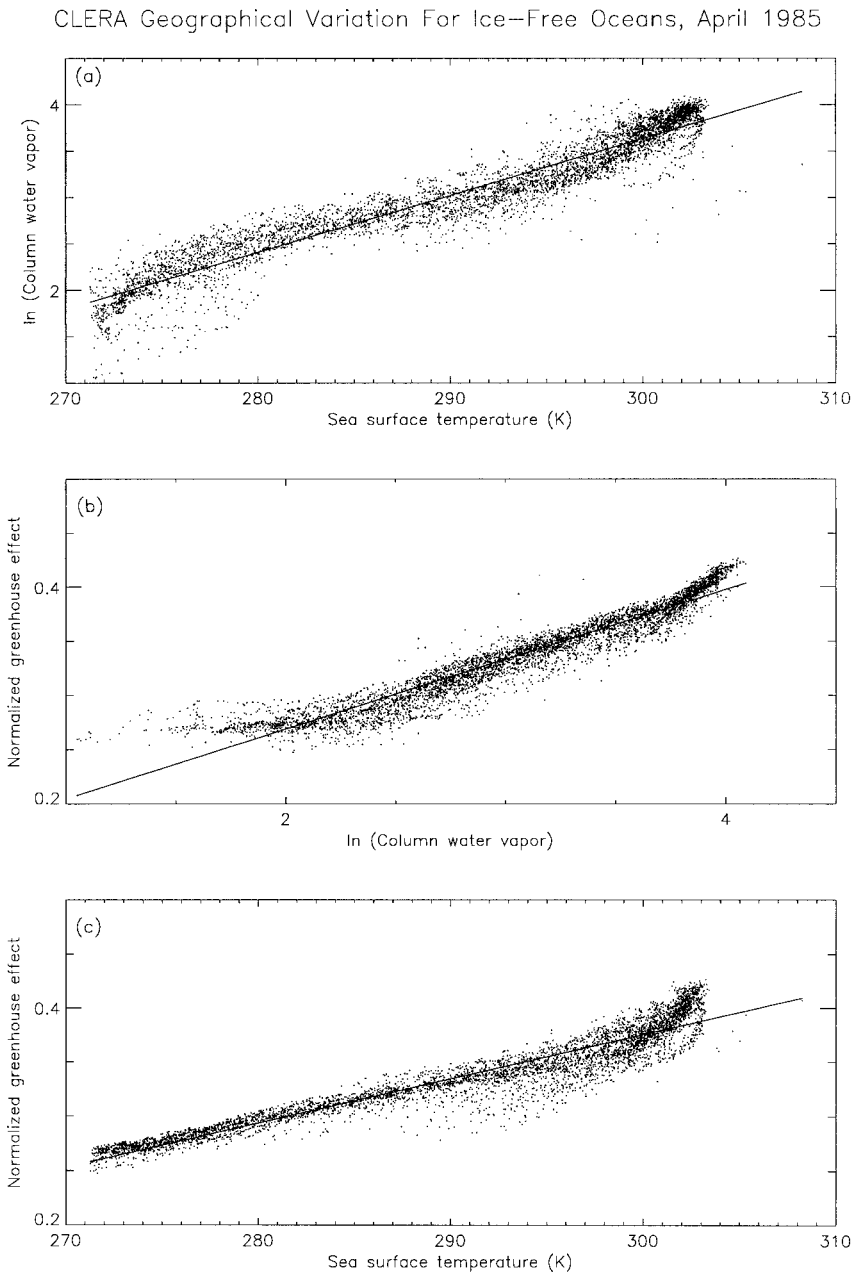

FIG. 1. Scatterplots and regression lines from the geographical distributions of CLERA data over the ice-free oceans for Apr 1985. (a) Natural logarithm of column water vapor (kg m^{-2}) against sea surface temperature (K). (b) Normalized greenhouse effect against natural logarithm of column water vapor (kg m^{-2}). (c) Normalized greenhouse effect against sea surface temperature (K).

We consider the results from the AMIP integration of HadAM3 initially, in order to illustrate the method. Figure 3 shows the relationships between the annual means of the column water vapor, normalized greenhouse effect, clear-sky outgoing longwave radiation (OLR) and surface temperature. The interannual variability of these quantities is very small (e.g., for surface temperature it is less than 0.4 K) and for this reason the column water vapor is shown on a linear scale on this and subsequent figures. Nevertheless, there are clear relationships between the quantities, which are discussed below. The correlation coefficients are given in Table 2, together with their level of significance. Throughout this paper, the significance levels take account of the statistical uncertainty in the correlations but not the physical uncertainty in the variables. Linear regression

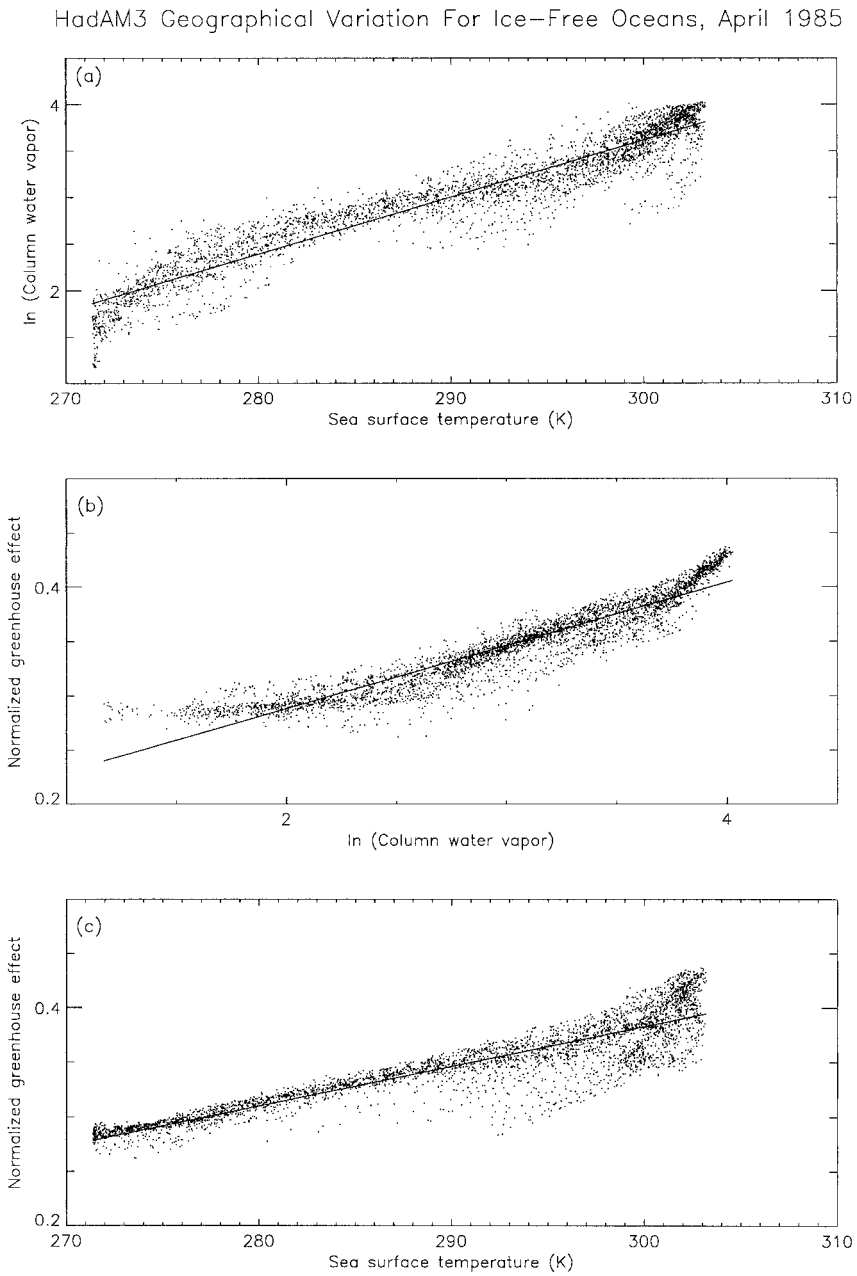

FIG. 2. As Fig. 1 but for data from an AMIP integration of HadAM3.

TABLE 1. Geographical regressions over ice-free oceans only.

	Linear least squares regression fit					
	$\ln W = a + b(\mathrm{SST})$		$g = a + b(\mathrm{SST})$		$g = a + b(\ln W)$	
Source	a	b	a	b	a	b
Raval and Ramanathan	−13.0	0.0553	0.658	0.00342	0.155	0.0576
Duval and Bréon	−15.4	0.064	—	0.004	0.045	0.0868
CLERA	−14.6	0.0614	−0.854	0.00410	0.140	0.0644
HadAM3	−14.8	0.0613	−0.709	0.00364	0.172	0.0581

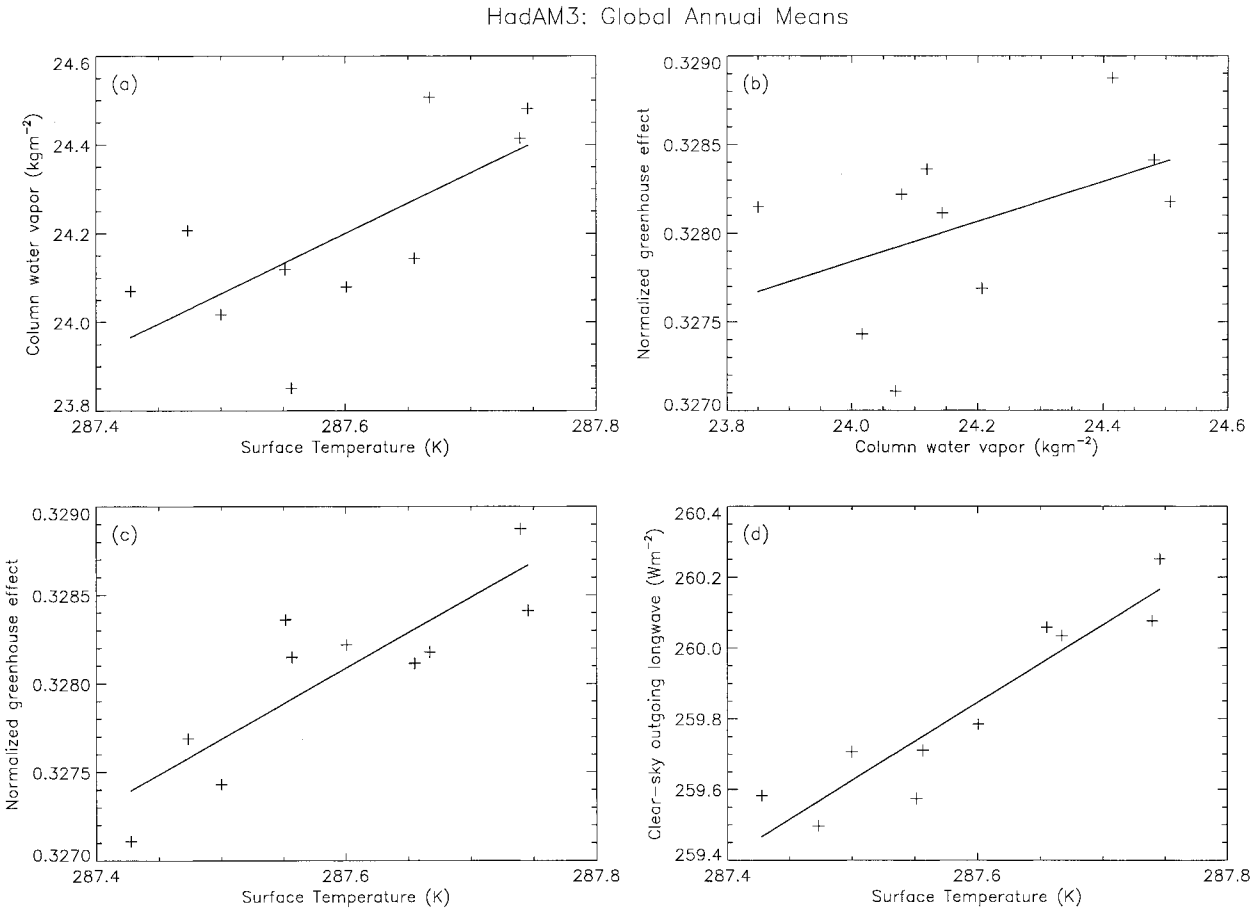

FIG. 3. Scatterplots and regression lines from the global, annual means of data from an AMIP integration of HadAM3 for 1979–88. The solid line shows the least squares regression. (a) Column water vapor (kg m^{-2}) against surface temperature (K). (b) Normalized clear-sky greenhouse effect against column water vapor (kg m^{-2}). (c) Normalized clear-sky greenhouse effect against surface temperature (K). (d) Clear-sky outgoing longwave radiation (W m^{-2}) against surface temperature (K).

TABLE 2. Global annual mean statistics. The ranges of uncertainty in the regression gradients define the 95% confidence intervals. The correlation coefficients (r) are given together with their level of significance.

Data source/model	Regression variables	Linear least squares gradient (y on x)	r	Significance (%)
CLERA	CWV, T_*	3.23 ± 1.91	0.71	99
	g, CWV	0.0011 ± 0.0012	0.50	90
	g, T_*	0.0031 ± 0.0059	0.30	60
	OLR$_c$, T_*	2.37 ± 2.51	0.49	90
HadAM3	CWV, T_*	1.36 ± 1.16	0.69	95
	g, CWV	0.0011 ± 0.0017	0.47	80
	g, T_*	0.0040 ± 0.0019	0.85	99
	OLR$_c$, T_*	2.20 ± 0.71	0.93	99
HadCM3 (control)	CWV, T_*	1.81 ± 0.20	0.89	99
	g, CWV	0.0019 ± 0.0003	0.82	99
	g, T_*	0.0044 ± 0.0004	0.91	99
	OLR$_c$, T_*	1.94 ± 0.16	0.93	99
HadCM3 (GHG)	CWV, T_*	1.78 ± 0.05	0.99	99
	g, CWV	0.0048 ± 0.0002	0.97	99
	g,T_*	0.0088 ± 0.0002	0.99	99
	OLR$_c$, T_*	0.18 ± 0.09	0.39	99

fits to the data were calculated using the method of least squares and the gradients and 95% confidence intervals are also shown in Table 2. Standard application of this method assumes that the values of the independent (x) variable are known precisely and that any uncertainty in the data is confined to the dependent (y) variable, so the regression is of y on x (Chatfield 1981). In this study, all the data are based on values extracted from reanalyses or GCM simulations, so it cannot be assumed that uncertainty exists only in one variable. In such circumstances it is usual to calculate two regression lines, those of y on x and x on y, with the difference providing a measure of the uncertainty in the regression (Chatfield 1981). In practice, we found that the x on y regressions added little to the uncertainty measure provided by the confidence intervals shown in Table 2, so for clarity they have been omitted.

To identify a water vapor feedback, we follow the method of Raval and Ramanathan (1989). Fundamental to the feedback is a clear positive dependence of CWV on surface temperature. Figure 3a shows a significant

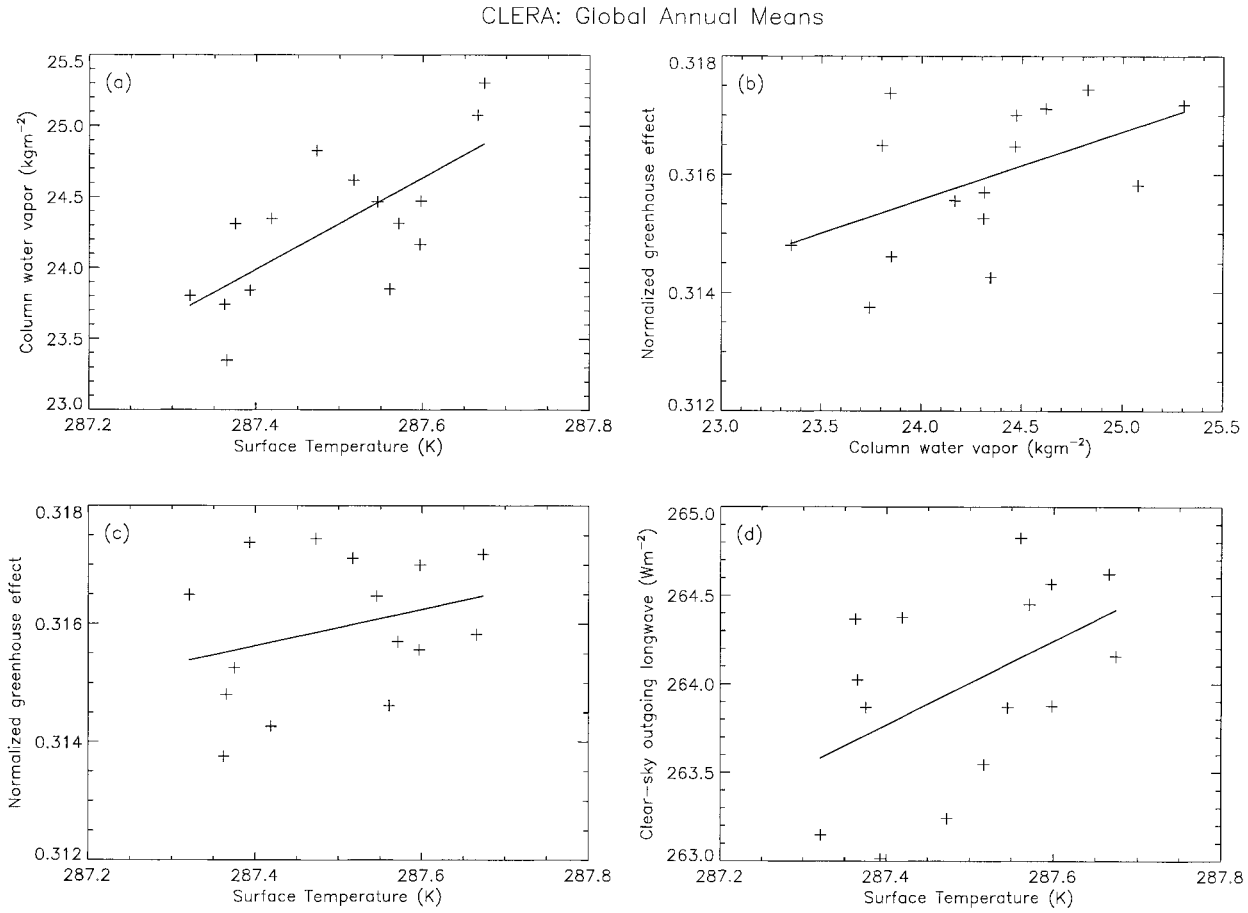

FIG. 4. Same as Fig. 3 but for CLERA data for 1979–93.

positive correlation between these variables, although there is considerable scatter about the regression line. The effect of the variations in CWV on the normalized clear-sky greenhouse effect is shown in Fig. 3b. Here the scatter is larger and the results less significant, although a positive dependence of g on CWV is nevertheless consistent with the expected feedback. However, it must be noted that changes in temperature lapse rate also influence g. Lapse rate changes may therefore potentially modify the inferred dependence of g on CWV. A further point relates to the scatter present in this figure. The global mean CWV is determined mainly by the water vapor amount at lower altitudes, particularly in the Tropics. Variations in g that are related to water vapor fluctuations at higher altitudes and higher latitudes may therefore not be accounted for by using CWV, despite their influence on g. These points will be revisited in section 4.

Evidence of a positive radiative feedback is provided by Fig. 3c, which shows a statistically significant increase of g with surface temperature at the rate of 4.0 $\times$ 10^{-3} K^{-1}, consistent with the values in Table 1. Finally, Fig. 3d shows a positive dependence of the clear-sky OLR on surface temperature. The regression gradient is calculated to be 2.20 W m^{-2} K^{-1} (Table 2), in good agreement with the values of 2.31 W m^{-2} K^{-1} from Raval and Ramanathan (1989) and 2.34 W m^{-2} K^{-1} from Cess et al. (1990). The blackbody dependence of the clear-sky OLR (OLR_c) on T_* may be approximated by (e.g., Cess 1989),

$$\frac{\partial \mathrm{OLR}_c}{\partial T_*} = \epsilon 4\sigma T_*^3, \tag{1}$$

where the earth's effective clear-sky emissivity is given by $\epsilon = \mathrm{OLR}_c/\sigma T_*^4$. For the HadAM3 global annual mean OLR_c of 260 W m^{-2} and mean surface temperature of 287.6 K, the blackbody $\partial \mathrm{OLR}_c/\partial T_*$ response equals 3.6 W m^{-2} K^{-1}. The regression gradient is significantly less than the blackbody response, indicating a positive clear-sky feedback consistent with the other correlations. The positive correlations between CWV, g, and surface temperature, and the slope of the relationship between the clear-sky OLR and surface temperature are characteristic of a positive water vapor feedback.

For the CLERA simulations, Fig. 4 shows more scatter than for HadAM3, although positive relationships do emerge from the regressions (Table 2). These show

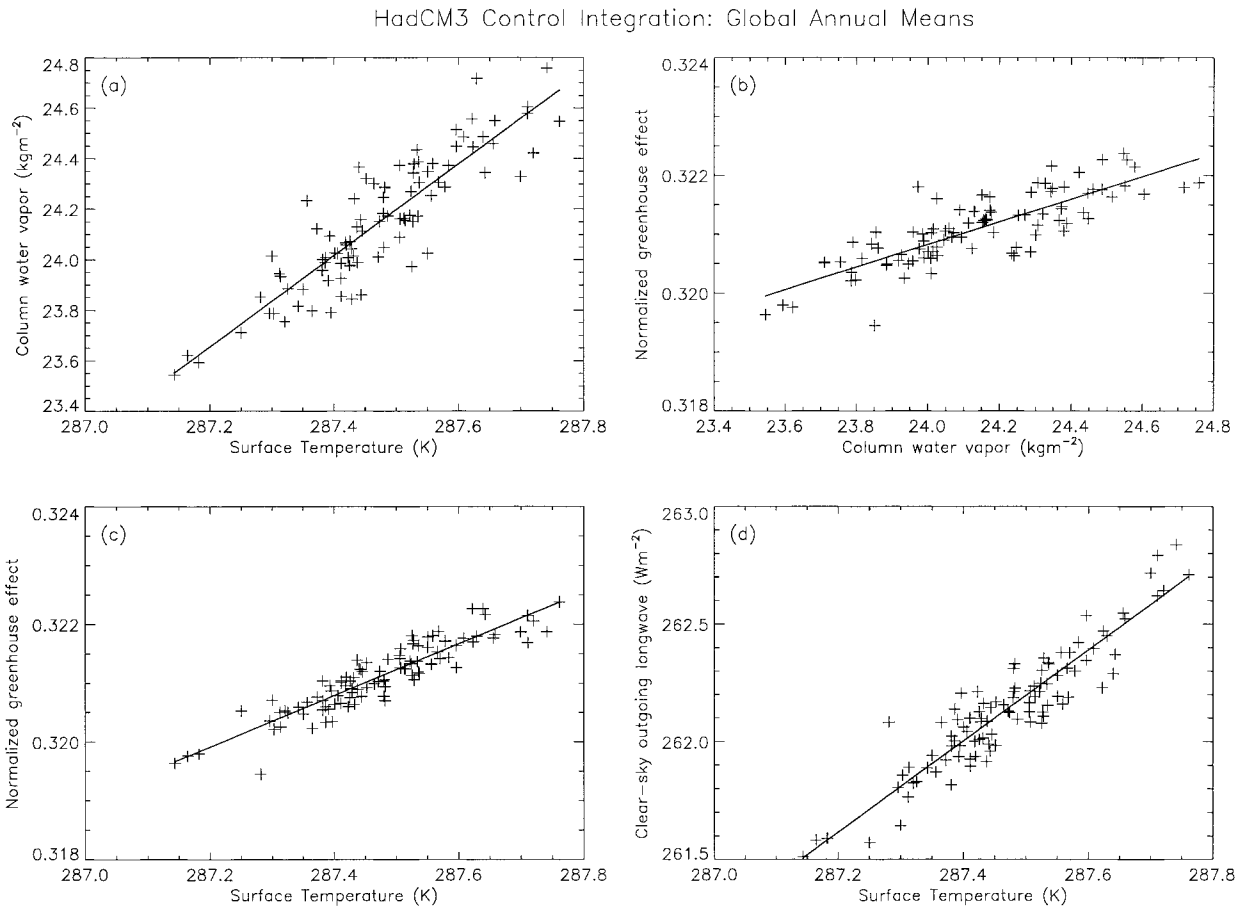

FIG. 5. Same as Fig. 3 but for data from the control integration of HadCM3.

a stronger dependence of the CWV on surface temperature than in HadAM3, though with considerable uncertainty. The regressions are also very noisy for the other variables, although the gradients are consistent with those from HadAM3. This observationally based estimate (albeit from an analysis in which the observations have been assimilated into a numerical model) thus supports the finding of a positive water vapor feedback in the HadAM3 results. Further analysis of the CLERA results is presented later.

Additional support for the value of $d\mathrm{CWV}/dT_*$ given by ERA was sought by comparing with data from the National Aeronautics and Space Administration Water Vapour project (NVAP) (Randel et al. 1996). NVAP provides an independent estimate of the column water vapor, through a blend of observations from the global radiosonde network, the SSM/I, and the TOVS. There are two major differences between the datasets. First, ERA assimilates the observations into the ECMWF weather forecast model, whereas NVAP uses a much simpler blending procedure. Second, NVAP includes the SSM/I data that are not used in ERA. There are only 6 complete years for which the datasets overlap (1988–93), so the comparison is unfortunately very noisy. In addition, no surface temperature information is available from NVAP, so the values from ERA were used. For this period, the global/annual means from ERA yield a value of $d\mathrm{CWV}/dT_*$ of 2.6 ± 2.6 kg m^{-2} K^{-1}, compared with 1.7 ± 2.7 kg m^{-2} K^{-1} from NVAP. The results are at least consistent, with the NVAP value being closer to that from the climate model, although the uncertainty in the slopes is very large.

For HadCM3 (Fig. 5), the use of a 100-yr record enables more of the natural variability of the model to be sampled, with the result that very clear correlations are apparent between these variables (Table 2). The scatter in the HadAM3 results means that it is difficult to make a definitive comparison between the atmosphere-only version (HadAM3) and the coupled model (HadCM3), although there seems to be fair agreement. It is worth noting that the slope of the regression of the clear-sky OLR on surface temperature in HadCM3 (1.94 W m^{-2} K^{-1}) is slightly lower than that from HadAM3 and the earlier work discussed above. At face value, this indicates a slightly stronger water vapor feedback in the coupled model. However, the difference is less than 10% and is not significant.

Last, Fig. 6 shows the corresponding results from the

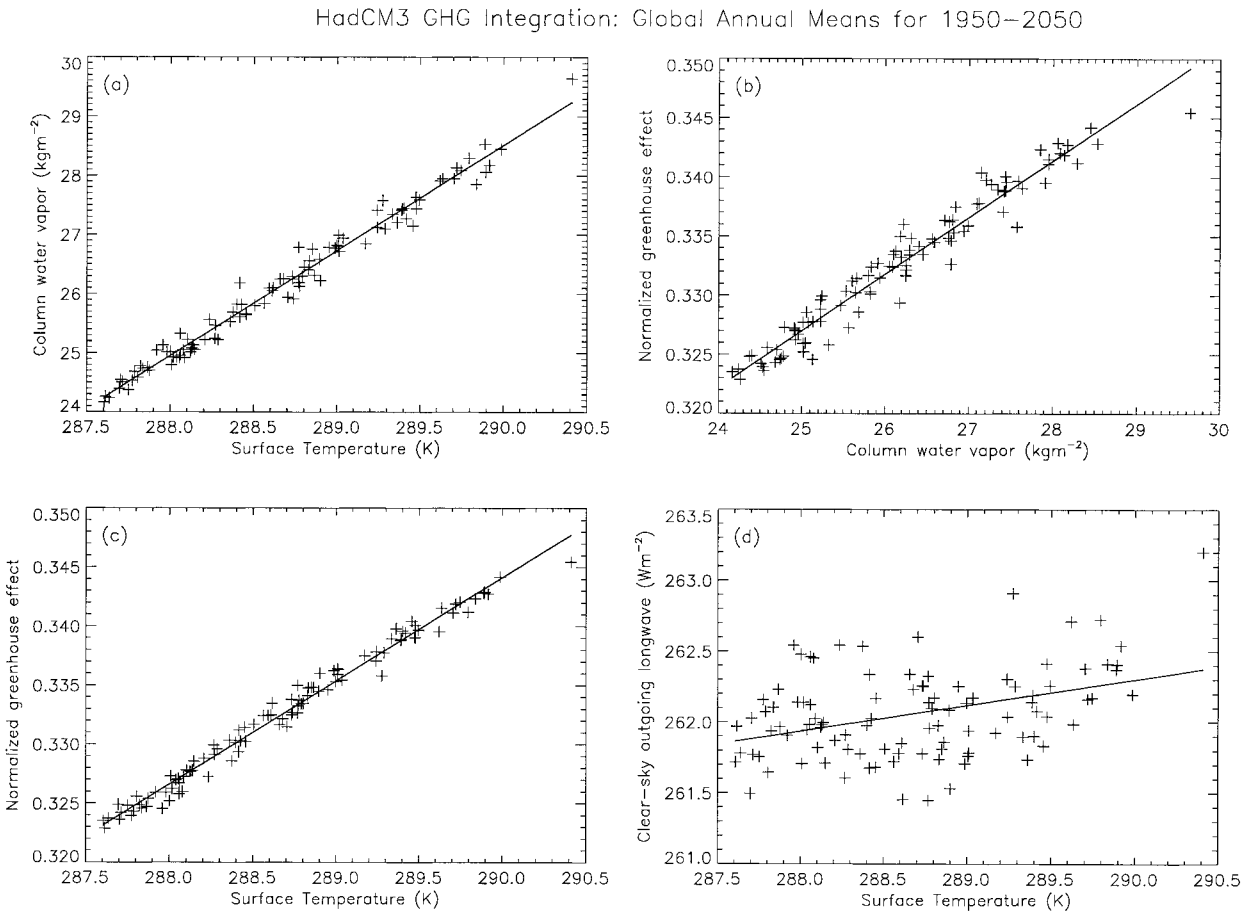

FIG. 6. Same as Fig. 3 but for data from the GHG integration of HadCM3 for 1950–2050.

GHG integration of HadCM3. The dependence of CWV on surface temperature is very similar to that in the control experiment (Table 2), suggesting that at least this element of the water vapor feedback operates in the same way in the GHG simulations as in the control, despite the much larger (and progressive) change in the SSTs in the GHG experiment. However, the slopes calculated for Fig. 6b–d are significantly different to those in the previous figures (see Table 2), because the radiative fluxes in the GHG experiment are influenced by the change in radiative forcing imposed during the 100-yr integration and the subsequent global warming. For example, the clear-sky OLR is almost independent of surface temperature (0.18 W m^{-2} K^{-1}). We show in section 4 that this behavior is due to the changes in greenhouse gases imposed through the integration. Increasing greenhouse gases acts to reduce the clear-sky OLR, which reduces the cooling to space and so leads to global warming (note that the temperature range in Fig. 6d is 3 K). The warming acts to increase the clear-sky OLR as the climate system tries to restore balance. In the GHG integration, these opposing factors almost cancel, so the clear-sky OLR hardly changes despite the 3 K global warming. This illustrates the futility of trying to observe the effects of global warming from space using only broadband radiation budget sensors; the roughly 0.5 W m^{-2} increase in the global mean clear-sky OLR through 100 yr of the GHG integration is several times lower than the errors associated with any feasible satellite monitoring system. Virtually all of the change in g evident in Fig. 6c comes about through the increase in surface temperature, rather than in the radiation budget at the top of the atmosphere. In order to diagnose the strength of the water vapor feedback in this integration it is therefore necessary to remove the signal from the greenhouse gases. This is discussed in the next section.

Given the HadAM3 and HadCM3 control integrations and the CLERA simulation, the broad agreement between the regressions suggests a consistent representation of the water vapor feedback. However, the confidence in this result is necessarily low, given the scatter in the regressions that use the CLERA annual means. We therefore investigated the possibility that more robust correlations for the CLERA results might be found by using all 180 monthly means from 1979 to 1993, as opposed to only the annual means. The seasonal signal

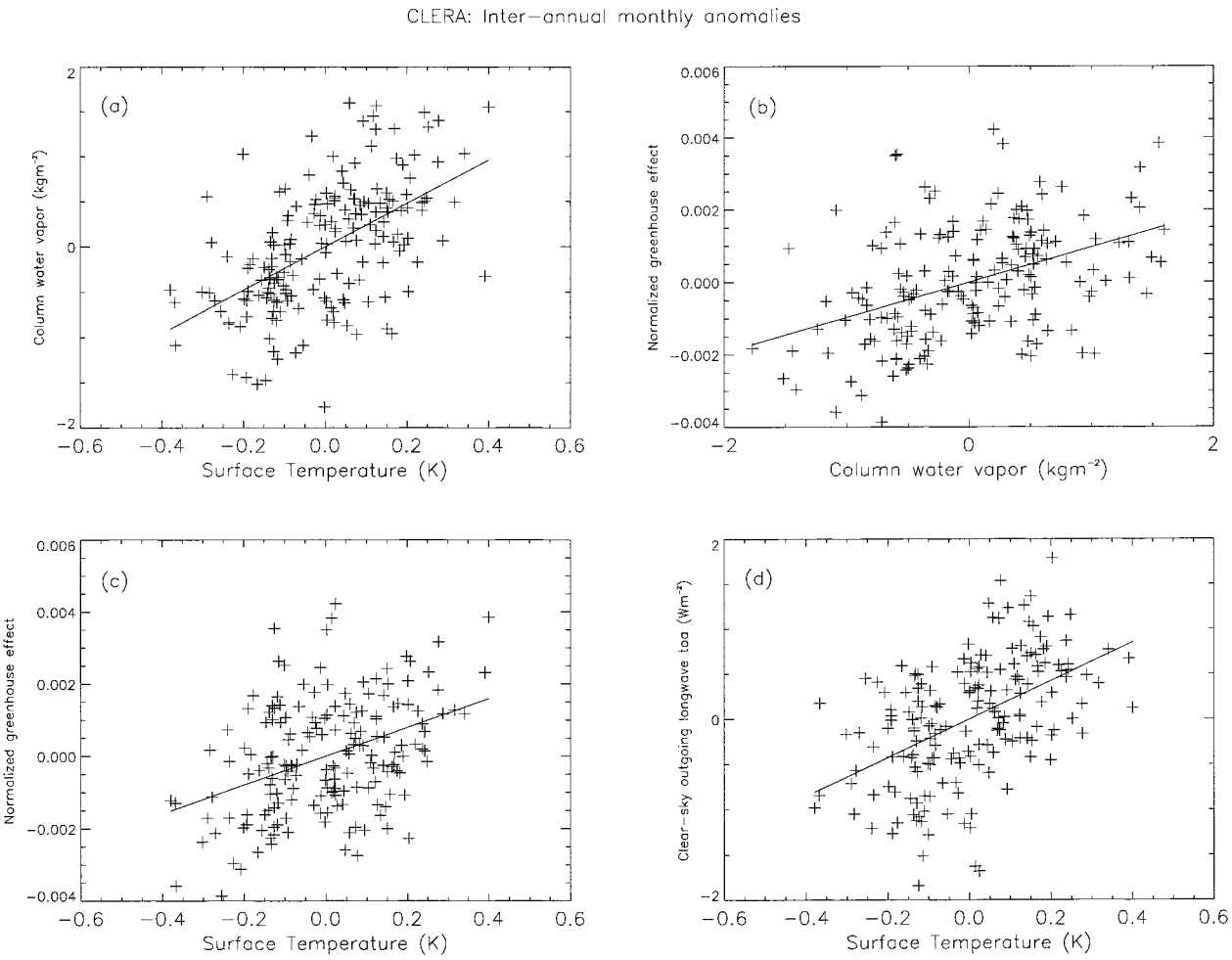

FIG. 7. Same as Fig. 3 but for interannual monthly anomalies of the data from CLERA for 1979–93.

was removed by calculating an interannual monthly anomaly (X'),

$$X'_{ij} = X_{ij} - \frac{1}{N}\sum_{j=1}^{N}(X_{ij}), \tag{2}$$

where X is a generic monthly mean variable (e.g., CWV), i is the month, j is the year, and $N = 15$ is the number of years of data. Relationships between the column water vapor, normalized greenhouse effect, clear-sky OLR, and surface temperature are shown in Fig. 7.

TABLE 3. The calculated timescale, t_0 (months), over which statistical independence is attained for interannual monthly anomalies of clear-sky OLR, column water vapor, and normalized greenhouse trapping. The degrees of freedom (d.f.) and required correlation coefficient to attain significant correlation at the 95% confidence level, r_{95}, are calculated from t_0.

	t_0	d.f.	r_{95}
OLR_c	10	19	0.43
CWV	12	15	0.48
g	7	26	0.38

As with the annual means, the variations are small and there is considerable scatter, although significant positive relationships between the variables are still apparent and it will be shown below that these are in reasonable agreement with the global mean analysis.

Correlations between the monthly interannual anomalies may overstate the statistical significance using the t test, due to autocorrelation of the independent variable (e.g., Yang and Tung 1998). To alleviate this problem, the timescale (t_0) over which statistical independence is attained may be estimated by

$$t_0 = \frac{1 + r_1}{1 - r_1}, \tag{3}$$

where r_1 is the correlation coefficient between the dependent variable and values time-lagged by one month. Due to the strong persistence of the variables studied, the number of degrees of freedom drops significantly from the maximum possible value of 178 (Table 3). The autocorrelation is largest for CWV, with the number of degrees of freedom only slightly larger than annual av-

TABLE 4. Regression gradient, correlation coefficient, and significance level for CLERA global mean monthly interannual anomalies of column water vapor (CWV), surface temperature (T_*), normalized greenhouse trapping (g), and clear-sky OLR (OLR_c).

Least squares linear regression			Correlation coefficient (r)	Significance level (%)
$d\text{CWV}/dT_*$	=	2.40 ± 0.55 kg m^{-2} K^{-1}	0.54	95
$dg/d\text{CWV}$	=	0.001 ± 0.0003 (kg m^{-2})$^{-1}$	0.43	95
dg/dT_*	=	0.004 ± 0.001 K^{-1}	0.40	95
$d\text{OLR}_c/dT_*$	=	2.13 ± 0.56 W m^{-2} K^{-1}	0.49	95

erage values. This raises questions as to the usefulness of using all 180 monthly means in regression analyses. However, applying the autocorrelation tests on annual mean values also reduces the effective sample size due to autocorrelation between years. The timescale for statistical independence of the monthly global means (t_0) is greater than the value of 4 months calculated by Yang and Tung (1998), who analysed tropical mean upper-tropospheric column water vapor from the NVAP dataset.

The regression gradients and correlation coefficients for the 180 monthly interannual anomalies using CLERA are displayed in Table 4. Considering the autocorrelation between dependent variables shown in Table 3, all regressions are significant at the 95% confidence level. The sensitivity of the normalized greenhouse trapping to column water vapor is consistent with the HadAM3 and CLERA annual mean regressions in Table 2. The normalized greenhouse trapping is calculated to increase with surface temperature at the rate 4.0×10^{-3} K^{-1}. The gradient is identical to the HadAM3 annual mean regression but larger than the corresponding regression applied to CLERA annual means. This is consistent with the gradient between clear-sky OLR and surface temperature of 2.13 W m^{-2} K^{-1} being less than the value calculated using CLERA annual means. The significance of these correlations adds weight to the regression analysis performed on the CLERA annual means. The broad agreement between the CLERA and climate model representations of the water vapor feedback strengthens the confidence in the model's ability to represent this mechanism. Nevertheless, this conclusion must be tempered by the scatter that is readily apparent in the figures and by a number of other uncertainties that are investigated in the following section.

4. Analysis of uncertainties

In this section we investigate some of the reasons for the differing estimates of the strength of the water vapor feedback obtained from the regression analysis of CLERA data and the various climate model experiments.

a. Radiative effect of increasing greenhouse gas concentrations

The CLERA simulations were performed by running a radiative transfer code (Edwards and Slingo 1996) using atmospheric temperature and specific humidity, surface temperature, and surface pressure data from ERA (Slingo et al. 1998). The effects of zonally meaned ozone varying on an annual cycle were also represented. Other radiatively important gases (CO_2, CH_4, N_2O, CFC11, and CFC12) were included; these were assumed to be well mixed in the atmosphere and their concentrations were allowed to increase linearly with time. The increase in the well-mixed greenhouse gases occurs in addition to the interannual variation of CWV and therefore acts to influence the variability of the normalized greenhouse effect. To determine whether this significantly affects the apparent strength of the water vapor feedback, the CLERA simulations were repeated using monthly mean ERA analyses for 1979–93. Two parallel sets of simulations were performed: one in which the well-mixed greenhouse gas concentrations were increased according to the original scenario and another in which the concentrations remained constant. Regressions were calculated on annual means formed from the two sets of results (Fig. 8, Table 5). The small differences between the gradients obtained with increasing trace gases in Table 5 and the values in Table 2 are due to the different temporal sampling of the ERA data; the original CLERA simulations were calculated from 6-hourly analyses, rather than monthly means. The increase in the gas concentrations leads to no change in the relationship between CWV and T_* (Table 5), since these two quantities are determined solely by the ERA data. However, the slope of g versus CWV is slightly larger and the slope of g versus T_* is slightly smaller than when the gas concentrations are fixed. In absolute terms, the changes in gradient are 3×10^{-4} W m^{-2} kg^{-1} and 2×10^{-4} W m^{-2} K^{-1}, respectively. The increase in greenhouse gases steepens the slope of the regression between the clear-sky OLR and surface temperature by about 0.06 W m^{-2} K^{-1}. These results indicate that the small increases in the well-mixed greenhouse gases during the ERA period (1979–93) have only a modest impact on the diagnosed strength of the water vapor feedback in CLERA. The difference between the two experiments is well within the estimated uncertainties in the gradients, shown as 95% confidence intervals in Table 5.

In contrast to the CLERA simulations, the much larger changes in the well-mixed greenhouse gases in the coupled model experiment GHG have a profound impact on the regressions (Table 2, Fig. 6). The scenarios used to define the changes in the concentrations in the HadCM3 GHG run and in CLERA are compared in Fig. 9. In GHG, carbon dioxide increases linearly between 1950 and 2020 and then increases by a compound factor of 0.65% per year until 2050. The concentrations of

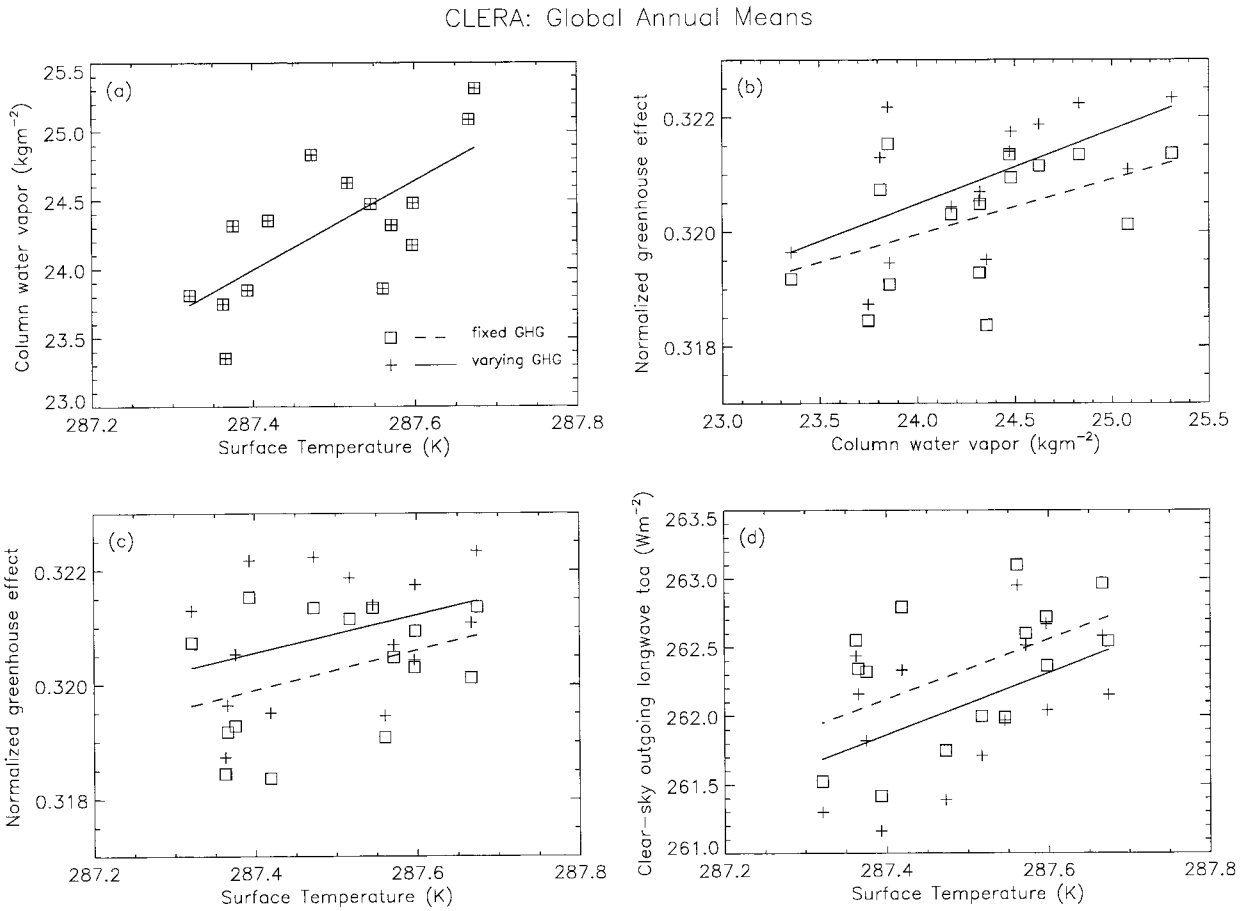

FIG. 8. Scatterplots and regression lines from CLERA illustrating the radiative effects of increasing well-mixed greenhouse gases. Solid lines show the regression fits to annual mean data with increasing greenhouse gases (data points indicated by plus symbols). Dashed lines show fits to data with greenhouse gas concentrations fixed at 1979 levels in the radiation code (data points indicated by open squares).

CFC11 and CFC12 are smaller than in CLERA between 1979 and 1993, and from 2005 onward they decrease. Overall, the concentrations of the well-mixed greenhouse gases change by a far greater amount during the hundred years of GHG, compared with the changes occurring over the comparatively short period of CLERA. To quantify the impact of these changes on the regressions and to establish whether it is still possible to diagnose the strength of the water vapor feedback in this integration, we performed a set of radiation simulations in which the annual mean temperature and humidity data at each grid point from GHG were processed using the Edwards–Slingo code, but with the concentrations of the well-mixed gases fixed at their 1950 levels. Figure 10 shows the results from these simulations, compared with the data from GHG, previously shown in Fig. 6. Fixing the concentrations makes no difference to the relationship between CWV and T_*, as in Fig. 8, but for the other panels the relationships largely revert to those found from the control experiment, in which the gas concentrations were also constant. The regression gradients (Table 5) are now much closer to those from the HadCM3 control run (Table 2). The differences between the slopes for GHG with the radiative effects of varying well-mixed gases removed and those for HadCM3 are 9×10^{-4} for g versus CWV, 7×10^{-4} for g versus T_*, and 0.266 for the clear-sky OLR versus T_*. These differences place the revised GHG regression lines only slightly outside the uncertainty ranges for HadCM3. The remaining discrepancies may be due in part to differ-

TABLE 5. Regression gradients for annual means with and without the radiative effects of varying concentrations of well-mixed greenhouse gases. The ranges of uncertainty define the 95% confidence intervals.

Source	Regression variables	Increasing greenhouse gases	Fixed greenhouse gases
CLERA	CWV, T_*	3.23 ± 1.91	3.23 ± 1.91
	g, CWV	0.0013 ± 0.0010	0.0010 ± 0.0011
	g, T_*	0.0033 ± 0.0055	0.0035 ± 0.0052
	OLR_c, T_*	2.25 ± 2.34	2.19 ± 2.24
HadCM3 (GHG)	CWV, T_*	1.78 ± 0.05	1.78 ± 0.05
	g, CWV	0.0048 ± 0.0002	0.0028 ± 0.0001
	g, T_*	0.0088 ± 0.0002	0.0051 ± 0.0001
	OLR_c, T_*	0.18 ± 0.09	1.67 ± 0.03

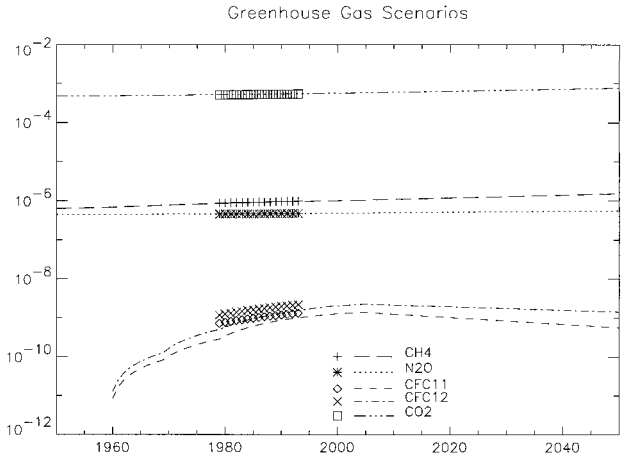

FIG. 9. The scenarios of changing greenhouse gas concentrations used in CLERA (symbols) and the HadCM3 GHG integration (lines). The IPCC IS95a scenario was used in the GHG integration.

ences in the temporal sampling of the data. The results in Table 2 were obtained using annual means calculated during the model integrations from 3-hourly calls to the model's radiation code. The fluxes in Table 5 were calculated outside the model from annual means of temperature and humidity and therefore have a sampling period of one year. Taking such uncertainties into account, these experiments suggest that the magnitude of the water vapor feedback in HadCM3 during global warming is very similar to that arising from the interannual variability in a fixed greenhouse gas simulation.

b. Effects of sampling over different surface types

Slingo et al. (1998) found that the land surface temperatures in ERA in regions such as Antarctica and the Northern Hemisphere continents do not agree well with in situ observations. The SSTs in ERA were taken from observations, but over land the surface temperatures were calculated by the numerical model. Similarly, in

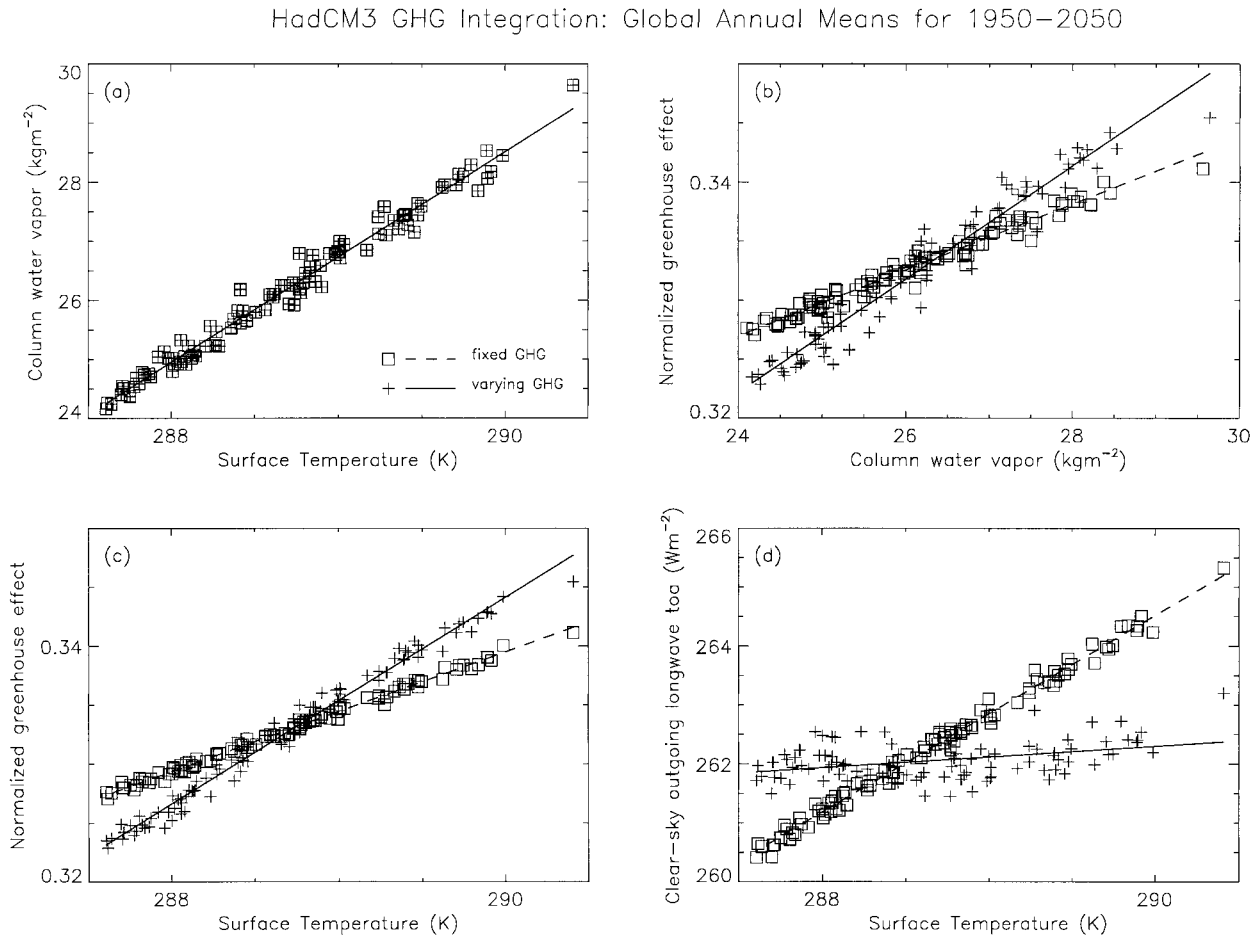

FIG. 10. Scatterplots and regression lines from the HadCM3 GHG integration, illustrating the radiative effects of increasing well-mixed greenhouse gases. Solid lines show the regression fits to annual mean data with increasing greenhouse gases (data points indicated by plus symbols), as shown previously in Fig. 6. Dashed lines show the fits to the data with the concentrations fixed at 1950 levels in the radiation code (data points indicated by open squares).

TABLE 6. Annual mean statistics for the global ice-free oceans. The ranges of uncertainty in the regression gradients define the 95 percent confidence intervals. The correlation coefficients (r) are given together with their level of significance.

Data source/model	Regression variables	Linear least squares gradient (y on x)	r	Significance (%)
CLERA	CWV, T_*	6.12 ± 4.33	0.65	99
	g, CWV	0.0010 ± 0.0011	0.47	90
	g, T_*	0.0053 ± 0.0115	0.27	60
	OLR_c, T_*	1.27 ± 4.94	0.15	40
HadAM3	CWV, T_*	1.69 ± 0.81	0.86	99
	g, CWV	0.0015 ± 0.0011	0.74	98
	g, T_*	0.0038 ± 0.0011	0.94	99
	OLR_c, T_*	2.03 ± 0.52	0.95	99
HadCM3 (control)	CWV, T_*	2.65 ± 0.39	0.82	99
	g, CWV	0.0011 ± 0.0003	0.68	99
	g, T_*	0.0047 ± 0.0006	0.86	99
	OLR_c, T_*	1.74 ± 0.23	0.83	99
HadCM3 (GHG)	CWV, T_*	3.39 ± 0.12	0.99	99
	g, CWV	0.0033 ± 0.0002	0.96	99
	g, T_*	0.0117 ± 0.0004	0.98	99
	OLR_c, T_*	−1.32 ± 0.18	−0.82	99

the AMIP run of HadAM3, SSTs were imposed as boundary conditions but land surface temperatures were calculated. The global mean surface temperatures in CLERA and HadAM3 therefore differ, so to determine whether this affects the estimated strength of the water vapor feedback, regressions were calculated using annual means for the ice-free oceans only (Table 6).

A comparison of the results in Tables 2 and 6 shows the effects of restricting the spatial sampling to the oceans. First, the gradient of the regression between CWV and T_* increases in all cases. This is to be expected because limiting the area to the ice-free oceans excludes the polar regions, where the dependence of CWV on T_* is weaker than in the Tropics. In addition, surface temperature variations are much smaller over the oceans than over the land. The response of CWV to increasing surface temperature may be limited in some land regions by the availability of soil moisture for evaporation and this may also contribute to the weaker gradients in Table 2. When ocean-only means are used, the gradients of g versus CWV are generally weaker than for the global means. This can be explained by the higher values of CWV over the oceans that cause g to be less sensitive to any further increases in water vapor. In all cases the variation of OLR_c with T_* is weaker using the ocean only means and, with the exception of HadAM3, the variation of g with T_* becomes stronger. This behavior is consistent with the higher values of $d\text{CWV}/dT_*$. The weaker increase of g with CWV over the oceans is overcome by the far stronger increase in the amount of CWV.

It is clear from Tables 2 and 6 that the water vapor feedback in both the control and GHG runs of HadCM3 is stronger when only ocean points are considered. For CLERA and HadAM3 the 95% confidence intervals in Table 6 encompass the slopes obtained using global data. The converse is also true, with the exception that the confidence interval on $d\text{CWV}/dT_*$ for CLERA in Table 2 does not contain the slope in Table 6. Thus, the complete removal of sea ice and land points from the global means does not lead conclusively to a different estimate of the magnitude of the water vapor feedback, despite the physical reasons for expecting it to be stronger over the oceans. This suggests that possible errors of a few degrees in the modeled temperatures of some land points are unlikely to cause significant errors in the estimates of the global water vapor feedback strength.

c. Height-dependent humidity response

Regression analysis of the various climate model experiments and ERA has shown broad consistency in the strength of the water vapor feedback. While it is necessary to average over geographic detail in diagnosing such a feedback, it is important to examine the similarity between the height-dependent nature of water vapor response to surface temperature between the model experiments and ERA. To address this issue, vertical profiles of water vapor sensitivity to changes in surface temperature were calculated for global annual mean values using linear regression fits. Figure 11a shows such profiles for the absolute water vapor sensitivities. For positive changes in surface temperature, there is moistening throughout the troposphere for all the model experiments and ERA with the largest response generally apparent at lower altitudes. While there appear to be differences between the models and ERA, the range of values are within the calculated statistical uncertainty as denoted by horizontal error bars. The significant errors attached to HadAM3 and ERA are the result of the small quantity of data used to determine the sensitivities; the statistical uncertainty for HadCM3 and HadCM3 GHG are an order of magnitude less and are thus not shown.

It was previously argued, for example by Shine and Sinha (1991), that fractional (or relative) variations in water vapor mass mixing ratio are of greater relevence in diagnosing water vapor feedback than absolute changes (see also the following section). Thus, in Fig. 11b the sensitivity of fractional changes in specific humidity (q_f) to surface temperature, where q_f is the water vapor anomaly normalized by the time-mean specific humidity (q_m), are plotted for global annual mean values. All the models and data show a positive relation in the troposphere and are consistent within the range of uncertainty. The climate models exhibit remarkable similarity considering the various forcings involved, the greatest sensitivity being in the upper troposphere in agreement with previous studies (e.g., Watterson et al. 1999; Del Genio et al. 1991). A similar response between the model experiments and ERA is apparent in the upper troposphere (250–500 hPa) and near to the surface (900–1000 hPa). However, ERA shows several notable differences, an unequivocal explanation of

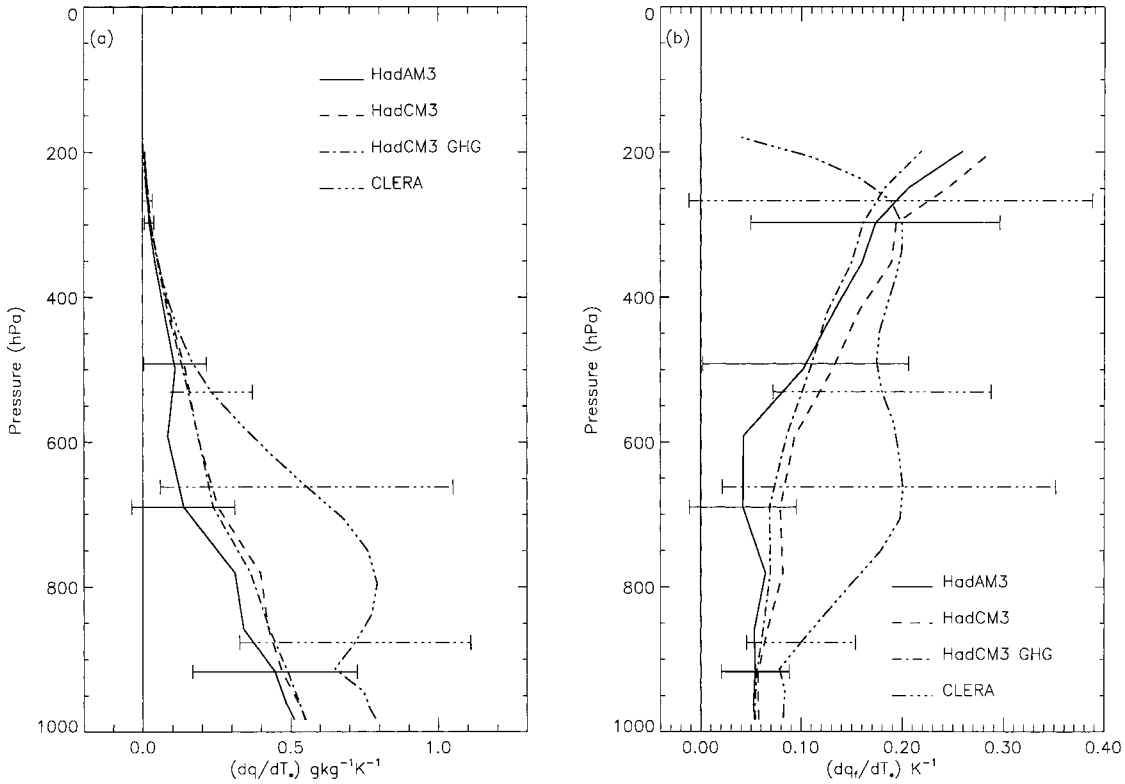

FIG. 11. Height-dependent humidity response for global annual means for (a) absolute changes in humidity and (b) relative changes. See section 4c for discussion.

which is beyond the scope of this paper. Several hypotheses are possible. The differences in the upper troposphere above about 250 hPa may be partly due to the tropopause height being lower in ERA than in the climate model. It is also known that the Hadley and Walker circulations are too intense in the climate model, and this may contribute to the stronger response in the upper troposphere to changes in surface temperature (Pope et al. 1999). The greater water vapor sensitivity calculated for ERA in the 500–850 hPa region is consistent with the observed similarity of $d\text{OLR}/dT_*$ and $d\text{OLR}/d\text{CWV}$ between CLERA and the climate model in Table 2, since the greater $d\text{CWV}/dT_*$ observed for ERA must be realized in a radiatively less significant region. The greater water vapor sensitivity of ERA in the 500–850 hPa region also has a high level of statistical uncertainty. When calculated using monthly mean values with the seasonal cycle removed, the sensitivity is reduced by about a quarter, which suggests that the midtropospheric peak in dq_f/dT_* for ERA is an overestimate. This is consistent with the value of $d\text{CWV}/dT_*$ calculated for interannual monthly anomalies being lower than the corresponding value calculated for annual means for ERA (Tables 2 and 4). Nevertheless, the variability of CWV in ERA is significantly larger than the climate model fluctuations for a given change in surface temperature and the reliability of such variations should be addressed in future studies. Preliminary comparisons with the NVAP data (section 3) hint at an overestimate in ERA moisture fluctuations, although the confidence in the NVAP data, which is limited by the spatial and temporal coverage of observations, must also be questioned. In conclusion, an important finding of this section is that for the model experiments and ERA, the sign and magnitude of the water vapor response to surface temperature throughout the troposphere agrees to within the, albeit large, statistical uncertainty.

d. Temperature lapse rate changes

Raval and Ramanathan (1989) argued that increases in normalized greenhouse trapping with CWV indicate a positive water vapor feedback, because changes in g are independent of surface temperature. As noted previously, g also depends on the temperature lapse rate. Raval and Ramanathan (1989) estimated changes in lapse rate to incur a 10% uncertainty in the value of dg/dT_*. This estimate was based on spatial changes in lapse rate that are small compared to the spatial variability of surface temperature. Over the interannual timescale there is no evidence to suggest that changes in temperature lapse rate incur a negligible contribution to dg/dT_*. To address this uncertainty, a further experiment was carried out using ERA monthly mean profiles

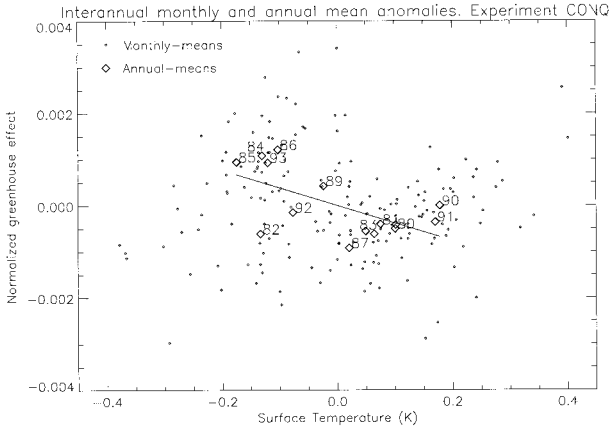

FIG. 12. Interannual anomalies of g and surface temperature for experiment CONQ. Dots represent interannual monthly anomalies and numbered symbols denote annual average anomalies with year number. The solid line is the regression between annual average anomalies.

but prescribing the specific humidity at the 15-yr mean value for each grid point and vertical level for the given month (experiment CONQ). For example, all Julys contain identical specific humidity values (q) that are calculated as

$$q_m(\theta, \phi, h)_j = \exp\left\{\frac{1}{15}\sum_{i=1}^{15} \ln[q(\theta, \phi, h)_{i,j}]\right\}, \quad (4)$$

where i denotes year, j is month, θ is latitude, ϕ is longitude, and h is the hybrid-vertical coordinate used in ERA. Geometric averaging was chosen due to the nonlinear effects of humidity on clear-sky OLR (e.g., Udelhofen and Hartmann 1995). Using monthly mean atmospheric profiles, Allan et al. (1999) showed that the interannual variability of the clear-sky OLR was within 3% of the variability calculated from the version of CLERA used in section 3 (experiment CTR), by considering the standard deviation of the global mean clear-sky OLR.

Using all 180 monthly mean values from CONQ, the correlation between the clear-sky OLR and surface temperature is significant at the 99% confidence level, assuming 14 degrees of freedom due to substantial autocorrelation of the data. A gradient of 4.0 W m^{-2} K^{-1} is similar to the estimated blackbody clear-sky OLR response of 3.7 W m^{-2} K^{-1} calculated using Eq. (1). This suggests that changes in lapse rate contribute only slightly to the clear-sky feedback. Indeed, there is no significant correlation between g and surface temperature for experiment CONQ using interannual monthly anomalies (Fig. 12). However, there remains a significant variability of g (more than $\pm 2 \times 10^{-3}$). This illustrates that while changes in temperature lapse rate do exert a significant influence on g, this variability is uncorrelated with surface temperature. Therefore the inferred water vapor feedback calculated in section 3 appears to be unaffected by lapse rate changes when considering interannual monthly anomalies.

When the regression is repeated using annual average values, a negative dependence of g on surface temperature is calculated for experiment CONQ, which is significant at the 95% confidence level (Fig. 12). An increase in clear-sky OLR with surface temperature of 5.3 W m^{-2} K^{-1} is calculated for CONQ, which is significantly greater than the sensitivity calculated using interannual monthly anomalies. For the control experiment, the sensitivity is similar for both the monthly and annual analysis. This suggests that changes in lapse rate may be significant when considering annual averages and the implied feedback is negative, with changes in atmospheric temperature acting to amplify the clear-sky OLR response to changes in surface temperature. Moreover, the magnitude of the positive water vapor feedback may be understated using the analysis of CLERA annual means in section 3. This is highly dependent on the quality of atmospheric and surface temperature and their interannual variability in ERA as well as the limited number of annual means.

e. A new moisture parameter

It is common to use CWV to infer water vapor variability (e.g., Raval and Ramanathan 1989). However, the parameter is strongly biased to lower altitudes and latitudes. For example, changes in water vapor amount in the upper troposphere, important in determining the clear-sky greenhouse effect (e.g., Soden and Fu 1995), are not captured by considering CWV variations.

To establish a meaningful relationship among atmospheric water vapor, surface temperature, and the clear-sky greenhouse effect it is necessary to employ a moisture parameter that samples regions of the atmosphere where water vapor fluctuations exert a significant radiative effect. Thompson and Warren (1982) demonstrated the strong dependence of clear-sky OLR on vertically averaged relative humidity. However, in highlighting water vapor feedback, the use of this parameter in the present study is limited. This is because the strong coupling between the water vapor concentration and atmospheric temperature, dictated by the Clausius–Clapeyron equation, means that the bulk of the positive water vapor feedback is acompanied by only small changes in relative humidity (e.g., Slingo and Webb 1997). Although it is important to establish that changes in relative humidity throughout the troposphere do not exert a significant effect on the water vapor feedback (e.g., Allan et al. 1999), a parameter that samples changes in water vapor concentration independent of temperature is required to present evidence of a water vapor feedback.

Using a radiative–convective model, Shine and Sinha (1991) showed that surface temperature is sensitive to 10% changes in water vapor mass mixing ratio, irrespective of the level in the troposphere at which the

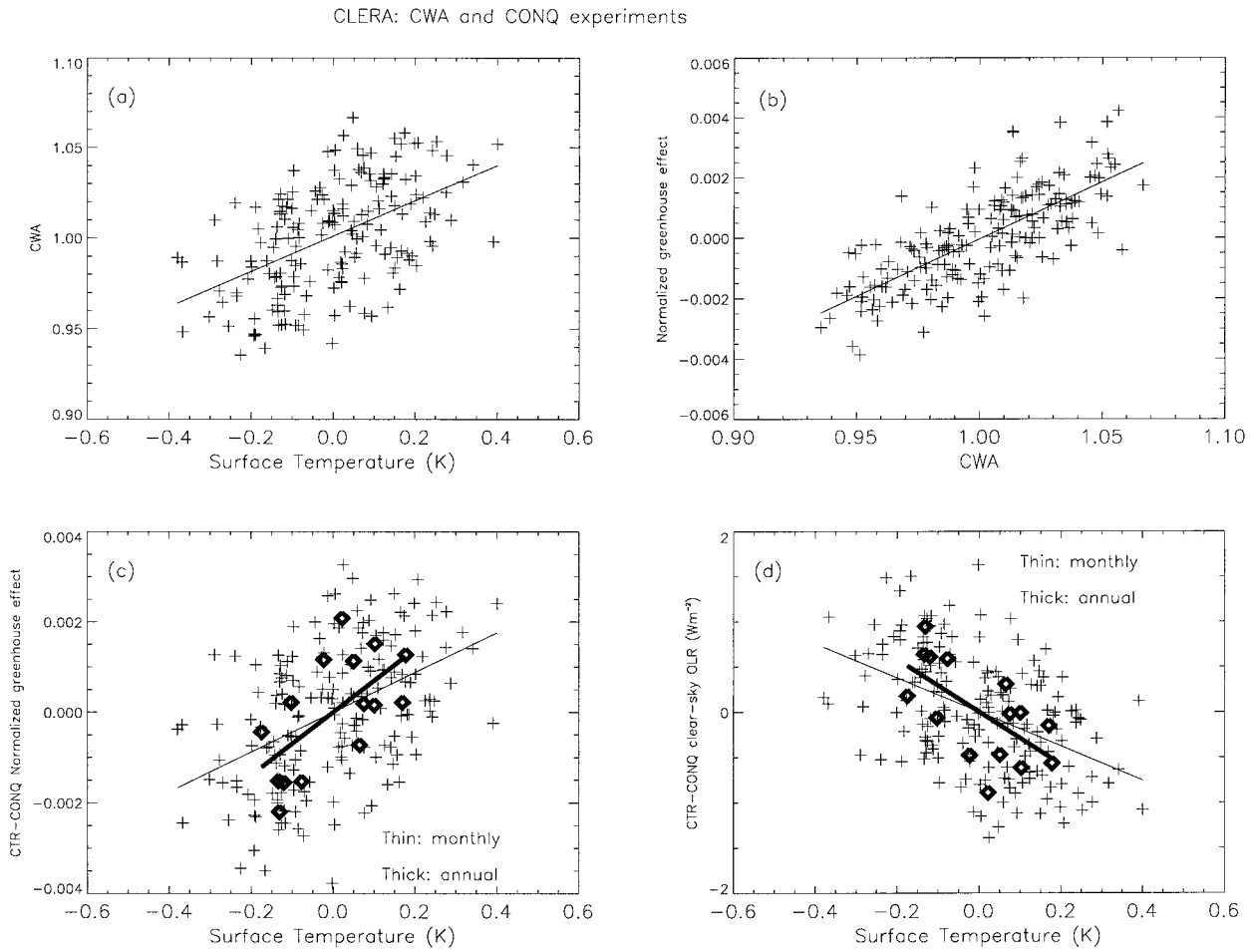

FIG. 13. Interannual monthly anomalies of (a) column water vapor anomalies (CWA) with surface temperature (T_*), (b) normalized greenhouse trapping with column water vapor anomalies (CWA), (c) the normalized greenhouse trapping difference (CTR − CONQ) with T_*, and (d) clear-sky OLR difference (CTR − CONQ) with T_*. Solid lines show the least squares fit regression line. Bold symbols in (c) and (d) denote annual averages; the bold lines represent the regression between annual average values.

moisture perturbation is applied. They further argued that observed moisture variations are consistent with percentage (or relative) changes in water vapor concentration that are uniform with altitude. It is therefore logical to use a moisture parameter that captures such relative changes in water vapor concentrations throughout the troposphere. Column mean relative changes in water vapor amount were calculated by vertically averaging the fraction, $\langle q(h)\rangle/\langle q_m(h)\rangle$, where $\langle q(h)\rangle$ is the global mean profile of specific humidity for a given month. The quantity $\langle q_m(h)\rangle$ is the global mean profile of the 15-yr monthly mean specific humidity given in (4). Global horizontal averaging was computed geometrically due to the nonlinear dependence of clear-sky OLR on q. This reduces the bias of global mean q to tropical moisture. The global average column mean water vapor anomalies were computed as

$$\mathrm{CWA}_{i,j} = \frac{1}{p_0 - p_t}\int_{p_t}^{p_0} \frac{\langle q(\theta, \phi, h)\rangle_{i,j}}{\langle q_m(\theta, \phi, h)\rangle_j}\, dp(h), \quad (5)$$

where i denotes year, j denotes month, with p_t and p_0 denoting the top and bottom pressure level over which vertical averaging is calculated. Vertical averaging of the relative water vapor anomalies weighted with the slab pressure-thickness $dp(h)$ ensures that the moisture parameter is not biased toward low-level moisture anomalies.

Using $p_t = 100$ hPa and $p_0 = 950$ hPa, the regressions shown in Figs. 7a,b are reproduced using the CWA parameter (Figs. 13a,b). Positive correlation between CWA and surface temperature is significant at the 95% confidence level, assuming 16 degrees of freedom using Eq. (3). The proposal of Lindzen (1990) that free-tropospheric humidity will diminish in response to surface warming is not apparent. Averaged globally throughout the troposphere, relative changes in specific humidity appear to be positively coupled with surface temperature, at least for the ERA climate (Fig. 13a). The value of CWA in explaining variations in atmospheric greenhouse trapping is highlighted by the strong, positive

TABLE 7. Regression gradient, correlation coefficient, and significance levels for global mean column water vapor anomalies (CWA), surface temperature (T_*), normalized greenhouse trapping differences, CTR − CONQ (Δg), and OLR_c differences, CTR − CONQ (ΔOLR_c). Values are calculated for interannual monthly anomalies and for annual averages (within parentheses).

Least squares linear regression	r	Significance level %
$d\text{CWA}/dT_* = 0.097 \pm 0.025$ (0.137 ± 0.102) K^{-1}	0.51 (0.59)	95 (95)
$dg/d\text{CWA} = 0.038 \pm 0.005$ (0.040 ± 0.015)	0.73 (0.83)	99.9 (99.9)
$d\Delta g/dT_* = 0.0044 \pm 0.001$ (0.0069 ± 0.0052) K^{-1}	0.46 (0.62)	90 (95)
$d\Delta\text{OLR}_c/dT_* = -1.9 \pm 0.53$ (-2.9 ± 2.17) $\text{W m}^{-2}\ \text{K}^{-1}$	−0.47 (−0.63)	90 (95)

correlation (significant at the 99.9% confidence level assuming 26 degrees of freedom) between g' and CWA displayed in Fig. 13b.

To ascribe further the changes in g to a positive water vapor feedback, the difference between interannual monthly anomalies of g between experiments CTR and CONQ are plotted with surface temperature anomalies in Fig. 13c. The differences in g between experiments CONQ and CTR are entirely due to interannual moisture fluctuations, thereby highlighting the positive water vapor feedback with the additional lapse rate signal removed. Similarly the differences in clear-sky OLR anomalies between CTR and CONQ show a negative dependence on surface temperature, also illustrating a positive water vapor feedback. However, strong autocorrelation within the samples render these relationships insignificant at the 95% confidence level. By annual averaging of the data (bold symbols) correlation is significant at the 95% confidence level assuming 13 degrees of freedom, albeit with steeper gradients than the monthly analysis. The regression gradients and correlation coefficients are displayed in Table 7 (annual average values are within parentheses).

5. Discussion

The purpose of this study was to investigate the possibility that useful information on the water vapor feedback could be obtained from the interannual variability of global mean quantities. We argued that such information should give a more reliable indication of the feedback operating on timescales relevant to global warming than that derived from geographical distributions or seasonal variations of the same quantities. In the absence of sufficiently reliable global satellite datasets, we used our previous CLERA simulations of the clear-sky greenhouse effect from the ECMWF reanalyses project (Slingo et al. 1998) to provide estimates of the feedbacks operating in the real world. We compared these with results from the latest version of the Hadley Centre Climate Model, including an AMIP integration of the atmosphere-only version forced by the observed SSTs (HadAM3) and also the coupled ocean–atmosphere version employed in climate prediction experiments (HadCM3). The ability to compare these two versions of the climate model with each other and with CLERA was particularly valuable.

Despite the considerable scatter in the data, we found evidence for a positive water vapor feedback in both the CLERA simulations (and hence the reanalysis data) and the climate model, consistent with earlier studies. There was no evidence for any significant difference between the magnitude of the feedback in the CLERA simulations and in the two versions of the climate model. Nevertheless, the results from the coupled model demonstrate that increases in the concentrations of greenhouse gases can significantly distort the relationships between the key variables if long time series are used, because trends in surface temperatures can take place despite no significant change in the top of atmosphere radiation budget. Over the 15-yr timescale of the ECMWF reanalysis, this effect produces only a small error in the diagnosed water vapor feedback, but over the century timescale of the greenhouse gas integration with the coupled model the impact is substantial. This effect must therefore be taken into account in the analysis of future satellite and synthetic radiation budget data that are obtained over periods longer than a decade or so.

Bearing in mind the arguments advanced in this paper in favor of using global means to infer the water vapor feedback, as opposed to the geographical distributions, it is nevertheless noteworthy that the two methods give similar estimates for the magnitude of the feedback. The implication is that the global variability examined here, including the systematic warming in the GHG climate prediction experiment, corresponds to all the points on plots such as Figs. 1 and 2 moving in the direction shown by the regression lines. However, changes in the atmospheric circulation and hence in the moisture distribution should perturb this simple picture, particularly in the Tropics. This merits further study.

The ECMWF reanalysis project made as much use of satellite data as was possible at that time, which is obviously crucial for studies that are strongly dependent on the quality of humidity information in the upper troposphere. Nevertheless, not all the available sources of humidity data were used and there were inevitably errors and deficiencies in the assimilation model that affected the CLERA simulations. These limitations will be addressed by a new reanalysis project (''ERA-40''), which will also extend the period to cover 1958–99. Further studies of the clear-sky greenhouse effect and water vapor feedback are planned with these data. It

would be extremely interesting to apply the techniques employed here to the data from other reanalyses and indeed to other climate models. Additional satellite measurements of the earth's radiation budget with global coverage are also needed in order to provide independent confirmation from observations of the results of such studies.

Acknowledgments. This work was in part funded by the U.K. Department of the Environment, Transport, and the Regions under Contract PECD 7/12/37 and by the U.K. Public Meteorological Service Research and Development programme. We acknowledge the help of Tim Johns in accessing data from the HADCM3 control and GHG integrations and for his comments, as well as those of the reviewers, on the manuscript.

REFERENCES

Allan, R. P., K. P. Shine, A. Slingo, and J. A. Pamment, 1999: The dependence of clear-sky outgoing long-wave radiation on surface temperature and relative humidity. *Quart. J. Roy. Meteor. Soc.*, **125,** 2103–2126.

Arrhenius, S., 1896: On the influence of carbonic acid in the air upon the temperature of the ground. *Philos. Mag. Series 5,* **41,** 237–276.

Bony, S., K.-M. Lau, and Y. C. Sud, 1997: Sea surface temperature and large-scale circulation influences on tropical greenhouse effect and cloud radiative forcing. *J. Climate,* **10,** 2055–2077.

Cess, R. D., 1989: Gauging water-vapour feedback. *Nature,* **342,** 736–737.

——, and Coauthors, 1990: Intercomparison and interpretation of climate feedback processes in 19 atmospheric general circulation models. *J. Geophys. Res.,* **95,** 16 601–16 615.

Chatfield, C. R., 1981: *Statistics for Technology: A Course in Applied Statistics*. 2d ed. Chapman and Hall, 370 pp.

Cox, P. M., R. A. Betts, C. B. Bunton, R. L. H. Essery, P. R. Rowntree, and J. Smith, 1999: The impact of new land surface physics on the GCM simulation of climate and climate sensitivity. *Climate Dyn.,* **15,** 183–203.

Del Genio, A. D., A. A. Lacis, and R. A. Ruedy, 1991: Simulations of the effect of a warmer climate on atmospheric humidity. *Nature,* **251,** 382–385.

Duvel, J. P., and F. M. Bréon, 1991: The clear-sky greenhouse effect sensitivity to a sea surface temperature change. *J. Climate,* **4,** 1162–1169.

Edwards, J. M., and A. Slingo, 1996: Studies with a flexible new radiation code. I: Choosing a configuration for a large-scale model. *Quart. J. Roy. Meteor. Soc.,* **122,** 689–719.

Gates, W. L., 1992: AMIP: The Atmospheric Model Intercomparison Project. *Bull. Amer. Meteor. Soc.,* **73,** 1962–1970.

Gordon, C., C. Cooper, C. A. Senior, H. Banks, J. M. Gregory, T. C. Johns, J. F. B. Mitchell, and R. A. Wood, 2000: The simulation of SST, sea ice extents and ocean heat transports in a coupled model without flux adjustments. *Climate Dyn.,* **16,** 147–168.

Gregory, D., R. Kershaw, and P. M. Inness, 1997: Parametrization of momentum transport by convection. II: Tests in single-column and general circulation models. *Quart. J. Roy. Meteor. Soc.,* **123,** 1153–1183.

Inamdar, A. K., and V. Ramanathan, 1998: Tropical and global scale interactions among water vapor, atmospheric greenhouse effect, and surface temperature. *J. Geophys. Res.,* **103,** 32 177–32 194.

Johns, T. C., R. E. Carnell, J. F. Crossley, J. M. Gregory, J. F. B. Mitchell, C. A. Senior, S. F. B. Tett, and R. A. Wood, 1997: The second Hadley Centre coupled ocean–atmosphere GCM: Model description, spinup and validation. *Climate Dyn.,* **13,** 103–134.

Lau, K.-M., C.-H. Ho, and M.-D. Chou, 1996: Water vapor and cloud feedback over the tropical oceans: Can we use ENSO as a surrogate for climate change? *Geophys. Res. Lett.,* **23,** 2971–2974.

Lindzen, R. S., 1990: Some coolness concerning global warming. *Bull. Amer. Meteor. Soc.,* **71,** 288–299.

Manabe, S., and R. T. Wetherald, 1967: Thermal equilibrium of the atmosphere with a given distribution of relative humidity. *J. Atmos. Sci.,* **24,** 241–259.

McNally, A. P., and M. Vesperini, 1996: Variational analysis of humidity information from TOVS radiances. *Quart. J. Roy. Meteor. Soc.,* **122,** 1521–1544.

Mitchell, J. F. B., T. C. Johns, and C. A. Senior, 1998: Transient response to increasing greenhouse gases using models with and without flux adjustment. Hadley Centre Tech. Note 2, Hadley Centre for Climate Prediction and Research, 15 pp. [Available from Hadley Centre, The Met. Office, Bracknell, Berkshire RG12 2SY, United Kingdom.]

Pope, V., M. Gallani, P. Rowntree, and R. Stratton, 2000: The impact of new physical parametrizations in the Hadley Centre climate model: HadAM3. *Climate Dyn.,* **16,** 123–146.

Randel, D. L., T. H. Vonder Haar, M. A. Ringerud, G. L. Stephens, T. J. Greenwald, and C. L. Combs, 1996: A new global water vapor dataset. *Bull. Amer. Meteor. Soc.,* **77,** 1233–1246.

Raval, A., and V. Ramanathan, 1989: Observational determination of the greenhouse effect. *Nature,* **342,** 758–761.

Shine, K. P., and A. Sinha, 1991: Sensitivity of the earth's climate to height-dependent changes in the water vapour mixing ratio. *Nature,* **354,** 382–384.

Slingo, A., and M. J. Webb, 1997: The spectral signature of global warming. *Quart. J. Roy. Meteor. Soc.,* **123,** 293–307.

——, J. A. Pamment, and M. J. Webb, 1998: A 15-year simulation of the clear-sky greenhouse effect using the ECMWF reanalyses: Fluxes and comparisons with ERBE. *J. Climate,* **11,** 690–708.

Soden, B. J., 1997: Variations in the tropical greenhouse effect during El Niño. *J. Climate,* **10,** 1050–1055.

——, and R. Fu, 1995: A satellite analysis of deep convection, upper-tropospheric humidity, and the greenhouse effect. *J. Climate,* **8,** 2333–2351.

Stephens, G. L., and T. J. Greenwald, 1991: The earth's radiation budget and its relation to atmospheric hydrology. I. Observations of the clear sky greenhouse effect. *J. Geophys. Res.,* **96,** 15 311–15 324.

Thompson, S. L., and S. G. Warren, 1982: Parameterization of outgoing infrared radiation derived from detailed radiative calculations. *J. Atmos. Sci.,* **39,** 2667–2680.

Udelhofen, P. M., and D. L. Hartmann, 1995: Influence of tropical cloud systems on the relative humidity in the upper troposphere. *J. Geophys. Res.,* **100,** 7423–7440.

Uppala, S., 1997: ECMWF Re-Analysis Project Rep. 1, Observing system performance in ERA. European Centre for Medium-Range Weather Forecasts, Reading, United Kingdom, 261 pp.

Watterson, I. G., M. R. Dix, and R. A. Colman, 1999: A comparison of present and doubled CO_2 climates and feedbacks simulated by three general circulation models. *J. Geophys. Res.,* **104,** 1943–1956.

Yang, H., and K. K. Tung, 1998: Water vapor, surface temperature, and the greenhouse effect—A statistical analysis of tropical-mean data. *J. Climate,* **11,** 2686–2697.